David P Gervais, Nicholas Foote

Recombinant deamidated mutants of Erwinia chrysanthemi L-asparaginase have similar or increased activity compared to wild- type enzyme, *Molecular Biotechnology*, vol. 56 , no. 10.

DOI : 10.1007/s12033-014-9766-9

PhD by Published Work

Statement of contribution by David Paul Gervais

Paper to be considered as part of the PhD by Published Work:

Gervais D, Foote N. Recombinant deamidated mutants of *Erwinia chrysanthemi* L-asparaginase have similar or increased activity compared to wild-type enzyme. *Molec Biotechnol* 2014; DOI 10.1007/s12033-014-9766-9.

Background: Deamidation is an important post-translational modification of *Erwinia chrysanthemi* L-asparaginase (Erwinase) which may happen during processing or storage of the enzyme. Deamidation is of interest to the regulatory bodies (US FDA) and the impact of deamidation on the enzyme is not well understood. Isolation of deamidated enzyme from the bulk enzyme preparations is tedious and non-trivial.

Contribution of candidate: DP Gervais had the lead role in this research. It was his idea to generate recombinant deamidated variants of Erwinase using heterologous protein expression in *E. coli*. DP Gervais designed the variants, and performed the protein expression, purification and characterisation including *in vitro* and *in silico* analyses. He also analysed the data and wrote the manuscript. DP Gervais served as the lead author and corresponded with the reviewers' comments. N Foote contributed the enzyme activity and K_m measurements.

I agree that David Paul Gervais made the aforementioned contribution to this paper.

Name	**Signature**	**Date**
Nicholas Foote	N. Foote	17th July 2014

Gervais D, Foote N. Recombinant deamidated mutants of *Erwinia chrysanthemi* L-asparaginase have similar or increased activity compared to wild- type enzyme. *Molecular Biotechnology* 2014; 56(10):865-877.

This paper is available digitally from the publisher (Springer) at DOI 10.1007/s12033-014-9766-9

Recombinant deamidated mutants of *Erwinia chrysanthemi* L-asparaginase have similar or increased activity compared to wild-type enzyme

David Gervais[*a], Nicholas Foote [a]

[a]Public Health England, Microbiology Services, Development & Production, Porton Down, Salisbury, Wiltshire, SP4 0JG, United Kingdom

*Corresponding Author. Tel : +44 1980 619595; fax: +44 1980 612694; email: dave.gervais@phe.gov.uk

Abstract

The enzyme *Erwinia chrysanthemi* L-asparaginase (ErA) is an important biopharmaceutical product used in the treatment of Acute Lymphoblastic Leukaemia. Like all proteins, certain asparagine (Asn) residues of ErA are susceptible to deamidation to aspartic acid (Asp), which may be a concern with respect to enzyme activity and potentially to pharmaceutical efficacy. Recombinant ErA mutants containing Asn to Asp changes were expressed, purified and characterised. Two mutants with single deamidation sites (N41D and N281D) were found to have approximately the same specific activity (1062 and 924U/mg respectively) as the wild type (908U/mg). However, a double mutant (N41D N281D) had an increased specific activity (1261U/mg). The N41D mutation conferred a slight increase in the catalytic constant (k_{cat} 657 s^{-1}) when compared to the WT (k_{cat} 565 s^{-1}), which was further increased in the double mutant, with a k_{cat} of 798 s^{-1}. Structural analyses showed that the slight changes caused by point mutation of Asn_{41} to Asp may have reduced the number of hydrogen bonds in this α-helical part of the protein structure, resulting in subtle changes in enzyme turnover, both structurally and catalytically. The increased α-helical content observed with the N41D mutation by circular dichroism spectroscopy correlates with the difference in $k_{cat,}$ but not K_m. The N281D mutation resulted in a lower glutaminase activity compared with WT and the N41D mutant, however the N281D mutation also imparted less stability to the enzyme at elevated temperatures. Taken as a whole, these data suggest that ErA deamidation at the Asn_{41} and Asn_{281} sites does not affect enzyme activity and should not be a concern during processing, storage, or clinical use. The production of recombinant deamidated variants has proven an effective and powerful means of studying the effect of these changes and may be a useful strategy for other biopharmaceutical products.

Keywords: deamidation; L-asparaginase; Erwinia; enzyme activity; enzyme mutations

1. Introduction

One of the mainstays used in clinical treatment of acute lymphoblastic leukaemia (ALL) is L-asparaginase (E.C. 3.5.1.1) [1]. Leukaemic cells require asparagine (Asn) to survive and proliferate, and L-asparaginase removes this essential nutrient by converting it to aspartic acid (Asp) [2]. Currently, there are two enzymes available for clinical use in the treatment of ALL: *Escherichia coli* L-asparaginase (EcA) and *Erwinia chrysanthemi* L-asparaginase (ErA). Historically, EcA has been the first treatment given clinically, but approximately 30% of patients develop a hypersensitivity to EcA, in which case ErA is utilised [3,4].

Like many enzymes in the asparaginase family, ErA is a 140,000Da homotetramer in its active form. ErA is a basic protein with an isoelectric point of pH 8.6 [5] and each subunit of the tetramer consists of 327 amino acids. The crystal structure of ErA has been solved to <1.8Å resolution [6, 7, 8] with a number of different substrates, and the enzyme overall structure has 222 symmetry and an active site mediated by residues Thr_{15}, Glu_{63}, Asp_{96}, Ser_{62}, Thr_{95} and Ala_{120} [6].

In common with many older biotechnology products, the manufacture of ErA is complex and lengthy. ErA continues to be the focus of an intensive effort to fully understand the complex process and further characterise the product [9]. In the manufacture of therapeutic enzymes, it is an important regulatory requirement to understand and characterise the main degradation and inactivation pathways that occur during protein expression, purification and storage. Such pathways generally involve oxidative

processes, protein-protein aggregation, and amino acid side chain modifications including deamidation.

Deamidation is probably the most difficult of these pathways to characterise, frequently occuring in proteins both *in vivo* and *in vitro* [10]. Deamidation is most common in Asn residues but is also possible in glutamine (Gln). The deamidation mechanism of an Asn side chain starts with the C-terminal α-nitrogen attacking the Asn side-chain carboxylate group, resulting in a cyclic succinimide intermediate and evolution of ammonia. The succinimide group is then hydrolysed to form a mixture of Asp and isoAsp [11]. A deamidation event leads to a lowering of the protein pI due to the change in residue charge from neutral to negative, leading to charge heterogeneity in protein products.

The overall effect of deamidation of a particular protein Asn residue may be deleterious to enzyme activity, structure or protein function [10,11]. In biopharmaceutical protein products such as monoclonal antibodies and ErA, deamidation may occur during manufacture or storage, and therefore must be characterised and monitored to understand if there is any impact on protein function. Limiting the amount of process-induced deamidation was studied recently for ErA [12], but the exact nature of the deamidated species, especially deamidation at particular sites, was not fully determined. The impact of a particular deamidation event is difficult to characterise fully. Understanding the impact of deamidation (and charge-variants in general) usually involves isolation using preparative HPLC and may be extremely laborious [13,14]. The isolated species may have multiple post-translational modifications, making it difficult to address the impact of a particular modification on protein or enzyme function. Finally, the HPLC-isolated charge variants may have a different stability profile, further complicating matters.

L-asparaginase is a good model for studying the effect of deamidation, as the activity of the enzyme depends on maintaining the quaternary structure. Thus, in addition to deamidation near the active site residues, deamidation that changes the affinity of the monomeric proteins may also affect enzyme activity. French and German researchers first studied EcA deamidation using isoelectric focusing in the 1970s [15,16,17]. More recently, researchers have used two-dimensional gel electrophoresis to separate post-translationally modified forms (including deamidated forms) of EcA and ErA [18].

In the present study, recombinant deamidated forms of ErA were produced, and characterised to understand the impact of asparaginyl deamidation on the physicochemical parameters and enzyme activity. A similar strategy has been employed [19, 20] to investigate the impact of particular deamidation sites on the structure and function of human lens αB-crystallin. The advantages and disadvantages of using this strategy to investigate charge variants of biopharmaceutically important proteins such as ErA is discussed.

2. Materials and Methods

Recombinant Protein Expression:

Reagents used were obtained from Sigma (Gillingham, UK) unless otherwise indicated. The *Erwinia chrysanthemi* NCPPB 1066 wild type gene [21] and deamidated mutants were synthesised by DNA2.0 (California, USA). Each mutant gene was sequence verified and inserted using NdeI and BamHI restriction sites into a pJ401 expression vector incorporating a T5 promoter [22, 23, 24, 25], kanamycin resistance gene, and lacI/lacO

repression system. The plasmids were stored at -20°C until needed, and transformed into the BL21 strain of *Escherichia coli* from New England Biolabs (Hitchin, UK) using a standard heat-shock protocol. Transformation cultures were grown overnight at 37ºC on Luria-Bertani (LB) agar selection plates containing 50µg/mL kanamycin sulphate. Single colonies were selected from the transformation plates and grown in 2L shake flasks (600mL working volume) at 37ºC in terrific broth (TB) with added 100µg/mL kanamycin sulphate and 5mM $MgCl_2$. Cultures were monitored for optical density at 600nm and upon reaching an OD_{600} in the range 0.6 – 1.0, were induced by addition of isopropyl β-D-1-thiogalactopyranoside (IPTG) to a final concentration of 1mM. Cultures were further grown post-IPTG addition overnight at 22 - 28ºC and harvested in a Beckman J-25 centrifuge and JLA-16250 (High Wycombe, UK) rotor at 4000rpm and 4ºC for 30min. Cell pellets were stored at -20ºC until needed for further processing.

Recombinant Protein Purification:

Isolation of the wild-type and mutant ErA enzymes was performed using a procedure modified from the methods of Kotzia *et al*. [26] and Lee *et al*. [27]. Briefly, cell pellets were reconstituted in 10mM sodium phosphate pH 7.5 containing 100mM NaCl and treated with protease inhibitor cocktail (SigmaFast, Sigma, Gillingham, UK). The cells were disrupted on ice using a SoniPrep150 (MSE, London, UK) in three 45s bursts. The disrupted lysate was cleared of debris using a Beckman J-25 centrifuge (High Wycombe, UK) and JA25-50 rotor at 11,000rpm for 45min at 4ºC. The cleared lysate was then applied to a L-Asn affinity column prepared and equilibrated as described previously, and eluted using a gradient of 10mM L-Asn in the equilibration buffer. Fractions were collected and pooled based on SDS-PAGE and extensively dialysed against 18.2MΩ water

in a 10kDa molecular-weight cut-off (MWCO) Snakeskin™ dialysis membrane (ThermoFisher, Loughborough, UK). The dialysate was concentrated using Amicon™ Ultra-15 regenerated cellulose 10kDa MWCO spin concentrators (Millipore, Watford, UK) and aliquotted for frozen storage at -20ºC.

Protein and Activity Assays:

The protein content of all samples described in this work was determined using a UV absorbance measurement with the known extinction coefficient for ErA, or using the method of Lowry [28]. The asparaginase activity assay was performed in borate buffer by measuring the decrease of the amide bond absorption of asparagine at 225nm as described previously [29]. The pH dependence of activity determined by using the 225nm assay in various buffers (phosphate or borate depending on the desired pH) and true system pH values were measured in the presence of substrate and enzyme. Analyses of the 225nm absorption of the buffer, substrate, and enzyme, each in isolation were conducted, to correct for any non-specific effects.

K_m and k_{cat} Determination:

Since absorbance changes for substrate concentrations in the region of K_m are too small to measure with the 225nm assay, the kinetic constants were determined by conducting enzyme reactions at various L-Asn substrate concentrations, with post-reaction derivatisation of the reaction product L-aspartic acid with 6-aminoquinolyl-N-hydroxysuccinimidyl carbamate (AQC). The derivatisation has the dual function of

stopping the enzyme reaction as well as allowing quantification of the labelled product by the use of UPLC with uv detection.

L-asparagine was added to 194 mM sodium borate pH 8.6 + 0.005% w/v bovine serum albumin (BSA) at 7.5, 12.9, 20, 30, 45, 70, 120 and 270 µM (chosen to give rate data at 10% intervals relative to V_{max}, based on a model with K_m set at 30 µM). Asparaginase samples were diluted in the same buffer containing 0.03% w/v BRIJ 35 to a calculated activity of 0.06 U/mL. A 9.9 mL aliquot of each substrate solution was equilibrated in a water bath to 37°C and 0.1 mL of sample was added. After a timed interval calculated to give approximately 10% substrate conversion at each concentration, 0.1 mL of the reaction mixture was withdrawn and mixed with 0.015 mL of AQC derivatisation reagent (AccQ-Tag Ultra; Waters Corp.) in a total recovery vial. This has been demonstrated to be sufficient to stop the reaction rapidly. Derivatised L-aspartic acid was then measured using a Waters Acquity UPLC system according to the manufacturers recommended protocol. L-aspartic acid dilutions were run as calibrants and results for the enzyme reactions were corrected for the initial presence of contaminating L-aspartic acid in the L-asparagine stock. K_m and V_{max} values were calculated by non-linear regression using GraphPad Prism 5 software. Values for k_{cat} were calculated from the V_{max} values by using the protein concentration determined by UV absorbance and a molecular weight per active site of 35,054 Daltons.

Glutaminase Assay:

An HPLC-based method for measuring glutaminase activity at pH 8.6 was used, similar to that described above for the K_m and k_{cat}. L-glutamine was used as the substrate at three concentrations (89, 243 and 463 µM). Low substrate concentrations were tested, because

previous experiments have shown apparent substrate inhibition for the glutaminase reaction of *Erwinia chrysanthemi* L-asparaginase. The enzymes were each added at the same measured asparaginase activity (final activity 0.061 U/ml) and reactions were run for a fixed time of 30 minutes at 37°C before derivatisation and HPLC measurement against known glutamate standards as described above. The maximum substrate conversion was 27%.

WCX Assay:

Samples were assayed for charge profile using a previously described weak cation exchange (WCX) HPLC method [12]. Briefly, a Dionex ProPac WCX-10 column (Dionex, Leeds, UK) was used with a gradient from 10 to 300mM sodium chloride in pH 6.2 sodium phosphate buffer, and absorbance data collected at a wavelength of 220nm.

Isoelectric Focusing:

Isoelectric focussing (IEF) of ErA samples was conducted using two separate techniques. In the first instance, Novex™ gels and running buffers from Invitrogen (Paisley, UK) were used to analyse the samples between the pH range 3-10. The IEF 3-10 gels were focused using a three step voltage protocol (100V for 1h, 200V for 1h, and 500V for 30min) and fixed in 12% trichloroacetic acid (TCA) before staining with Invitrogen SafeStain™. Samples were also analysed using Lonza IsoGel Agarose IEF plates in the pH range 7-11. Samples were electrophoretically focused using a Multiphor II (GE Healthcare, Amersham, UK) system at 1000V constant voltage with a power limit of 25W, using 0.01M glacial acetic acid as the anolyte and Cathode Fluid 10 (Serva, Heidelberg,

Germany) as the catholyte. Immediately upon removal of the voltage, the IEF plate was fixed in aqueous TCA containing methanol and sulphosalicylic acid. After fixing, the gel plate was thoroughly washed and dried and stained with Coomassie Brilliant Blue R-250 (Bio-Rad, Hemel Hempstead, UK) in a mixture of water, acetic acid and ethanol. Gels were imaged using a Bio-Rad GS-800 densitometer.

SDS-PAGE:

Analysis by SDS-PAGE was conducted using Novex™ 4-12% Bis-Tris gels from Invitrogen (Paisley, UK) with MES running buffer and Invitrogen Mark12™ ladder. The electrophoresis was conducted for 35min at 200V constant voltage and gels were stained in SafeStain from Invitrogen. Gels were imaged using a Bio-Rad GS-800 densitometer.

Enzyme Stability Experiments:

The effects of both thermal and denaturing stress on the enzymatic activity were assessed using methods adapted from Papageorgiou et al [30]. Briefly, for thermal stress, enzyme aliquots were diluted to 20 U/mL in 50mM sodium phosphate buffer pH7.2, mixed and incubated at a given temperature for 3min using a water bath. The enzyme aliquots were then stored on ice for at least 1h before measurement of activity using the UV assay described above. For denaturing stress experiments, 250U/mL enzyme stocks were diluted (16µl enzyme plus 144µl denaturant) with various concentrations of urea in 50mM sodium phosphate pH7.2. The enzymes were held at room temperature (23°C) for 1h in denaturant, then assayed for activity using the UV method described above. The UV assay uses a 1 in 100 dilution factor which was utilised as a rapid refolding step.

Circular Dichroism Analyses:

Circular dichroism (CD) analyses were performed using a Jasco J-715 spectropolarimeter at Alta Bioscience (Birmingham, UK). The analyses were carried out between 280 and 190nm, using samples were provided in analytical-grade water (AGW); a sample of AGW was used as a blank. The deconvolution of the spectra was performed using Dichroweb [31 - 33].

Molecular sequence and structure analyses:

Sequence alignments were performed using Clustal Omega [34] and depicted using Espript [35]. Molecular graphics and analyses were performed with the UCSF Chimera package [36]. Chimera is developed by the Resource for Biocomputing, Visualization, and Informatics at the University of California, San Francisco (supported by NIGMS P41-GM103311)

3.0 Results and Discussion

The manufacturing process for ErA has been discussed previously [9, 37] and has recently been the focus of on-going efforts to fully characterise the product and define the operating parameters for its production. During processing, oxidised, aggregated and deamidated species may be created. A key part of controlling the process is ensuring that these species are kept within certain limits, to ensure product consistency. Measurement of deamidated protein species may be made using the WCX HPLC assay, IEF, or mass spectrometry methods. However, quantitation of these species and understanding their impact on the final biopharmaceutical preparation are two separate matters. A full

understanding of the functional activity of deamidated proteins requires their isolation as relatively pure species. Deamidated species can be isolated using preparative HPLC techniques, but the isolated peaks often contain tiny amounts of protein, meaning many repeat injections to produce enough material for further study. Furthermore, the isolated species often contain multiple post-translational modifications, making understanding the impact of single modifications (i.e., deamidation at a particular site) difficult or impossible.

Therefore, the production of recombinant deamidated ErA species was determined as an appropriate strategy to attempt to understand their contribution or impact on efficacy in the clinical use of the enzyme. Likely ErA deamidation sites were identified using existing mass spectral data (data not shown), and the ErA sequence [21] was then analysed to determine which Asn residues were most likely to deamidate based on previous work in the literature [38, 39, 40]. The rate of deamidation depends on the amino acid residue on the C-terminal side of Asn, with Gly being the most reactive followed by Ala. Previous work had shown that Asn_{281} [12] is a likely candidate for deamidation with the sequence $N_{281}G_{282}$, even though, based on published crystal structures [6, 7, 8], its location lies buried inside the tetrameric assembly. When the available crystal structures were analysed using molecular modelling software a further candidate, Asn_{41} was identified, with the sequence $N_{41}A_{42}$. Asn_{41} is a particularly interesting site as it occupies a solvent-exposed position on the protein, regardless of whether the enzyme is assembled as a tetramer or in its monomeric state. This makes Asn_{41} potentially prone to deamidation at any time during its production, storage or use. The positions of both of these (Asn_{41} and Asn_{281}) potential deamidation sites (Figure 1A) are located away from the active site and were selected for further study as recombinant deamidated mutants. In comparison with other bacterial L-asparaginases (Figure 1B), ErA Asn_{41} is conserved in EcA and has high

similarity with Gln_{41} in the Erwinia carotovora L-asparaginase (EwA), while Asn_{281} is a Ser residue in both EcA and EwA. One important point to note regarding the recombinant deamidation strategy is the inability to produce deamidated protein containing iso-Asp residues, which are a product of the natural reaction but cannot be made by recombinant means.

Four versions of ErA were produced in this study: wild-type (WT) ErA, N41D, N281D and a double mutant, N41D N281D. Production of the recombinant proteins (Figure 2) was monitored using SDS-PAGE. The gel depicted is for the WT enzyme and is representative of the production of all four recombinant proteins, which were grown simultaneously in shake flasks. Final enzyme yields for the WT, N41D and N281D proteins were approximately 3.9 – 5.1mg/L culture, but the double mutant exhibited a markedly increased production of 10.3mg/L culture. Lysates from all of these preparations were analysed by SDS-PAGE and it appeared that the double mutant N41D N281D exhibited higher levels of production. It is not understood why this mutant may have expressed at higher levels. The final preparations of all four recombinant enzymes (Figure 3) appeared homogeneous as judged by SDS-PAGE.

The recombinant protein preparations were studied for charge differences using IEF. The IEF gels (Figure 4) were run in two ways, first on vertical gels with a wide pH range (3 – 10) and then on ultrathin agarose gels with a narrow pH range (7 - 11). The wide-range gel image demonstrates the relative homogeneity of each protein sample and the lack of contaminating bands in the low-pI region (<7), demonstrating that the samples contained the alkaline ErA variants and not the acidic EcA enzyme, which would have been present in small amounts in the host cell. Due to the wide pH range of this gel and the high pI of ErA, some of the protein bands appear very near or even at the level of the sample wells. Therefore, higher-resolution flat bed electrophoresis was performed in the more narrow

pH range between 7 and 11. This gel, also pictured in Figure 4, shows that the WT and N281D enzymes have roughly the same pI, as do the N41D and the double mutant. Interestingly, the contribution of the internal mutation N281D to the enzyme's pI is negligible, in the case of both the single mutant N281D and the double mutant N41D N281D.

Using the more sensitive WCX HPLC assay (Figure 5), subtle differences in charge variation can be observed. However, the general trend is that there are two groups of charged species, N281D and the WT enzymes forming one group, and N41D and the double mutant forming the second, with retention times only just after the HPLC void peak. The N41D and double mutant species have the largest charge differences to the WT enzyme, at -1 per monomer or -4 per tetramer. As discussed previously [12], the acidic (putative deamidated) species observed during routine manufacture of ErA elute at relative retention times (RRT) between 0.7 and 1.0 in this assay. These data taken together suggest that the species routinely observed in ErA clinical preparations are only marginally deamidated, and either have internal modifications (like N281D) or have fewer modifications per tetramer, e.g., only one monomeric subunit is deamidated per tetramer.

An important point to address regarding the deamidated mutants is whether they retain enzymatic activity. The activity of each mutant was tested in triplicate in borate buffer pH 8.6 at 37°C using L-asparagine as the substrate, and the data (Table 1) demonstrate that unexpectedly, the double mutant has a higher specific activity than the WT or single-mutant enzymes, which are all relatively similar. The glutaminase activity of the recombinant enzymes was also determined and found to be low compared to asparaginase activity. However, the internal mutation N281D appeared to correlate with a lower glutaminase activity in both the single (N281D) and double (N281D N41D) mutants compared with the WT and the N41D enzymes.

In order to further understand the differences observed in activity, the enzymatic catalytic constants K_m and k_{cat} for L-Asn were determined for each of the four recombinant enzymes (Table 2). Michaelis-Menten plots from these analyses (Figure 6) demonstrate the robustness of the kinetic data. The results confirmed the observations made from the native-substrate activity data, and demonstrate that an apparent synergistic effect of the two mutations (N41D and N281D) raises the catalytic performance of ErA beyond the WT or the corresponding single-mutant species. Mutation N281D appears to result in a decreased substrate affinity by a factor of 2, and this effect is also observed for the double mutant compared to the WT. Mutation N41D does not change the K_m value, but results in a marginally higher turnover number (657 vs 565 s^{-1}). However, the species with both mutations has even higher catalytic efficiency (798 s^{-1}). The possible reasons for this observed effect are discussed below.

The stability profiles of the ErA mutants were assessed in terms of enzymatic activity using comparative experiments adapted from Papageorgiou et al [30]. The results (Figure 7A) for the thermal stability study illustrated that both enzymes carrying the N281D mutation, internal to the quaternary structure, resulted in thermal inactivation at a lower temperature (approximately 43ºC and greater) than those without the mutation (≥56 ºC). Incubation of N281D and the double mutant at 49ºC for 3min resulted in loss of approximately 50% of enzymatic activity, while this temperature had no effect on the activity of the WT or N41D enzymes. The external mutation N41D appeared to have no effect on the enzyme stability, correlating well with the thermal stability profile of the wild type ErA. The residual enzyme activity after exposure to denaturing conditions was also examined, and similar to the thermal profiles, the N281D mutation resulted in an inability to refold after exposure to urea concentrations greater than 1.5M (Figure 7B), while the external N41D mutation had no impact on the stability of the enzyme. Linear enzyme

reaction curves were obtained in all cases (data not shown), suggesting that rapid enzyme refolding had occurred and not interfered with the activity results. These stability results correlate well with the K_m data in Table 2, suggesting that any structural differences caused by the N281D mutation, internal to the tetrameric structure, cause a decrease in substrate affinity as well as a decrease in the stability profile. After denaturation with urea, the ability of the enzyme to refold into the active, quaternary structure is affected, suggesting that N281 may play an important role in the folding pathway for this enzyme. Similar observations have been made for other multimeric, subunit enzymes with point mutations after denaturation in urea [41].

In order to ensure that the higher activity and enzymatic constants observed for the double mutant N41D N281D were not an artefact of a shifted optimum in the relationship between pH and activity, the relationship was investigated using the UV activity assay with substrate in buffers of various pH values between 6.5 and 10. The data (Figure 8) demonstrate that there is no gross difference in the pH versus activity relationship for the double mutant when compared with the WT. The data are presented as points, with a dynamic 4-parameter Gaussian fit also shown, calculated using SigmaPlot (Systat, California, USA).

As the increased catalytic performance of the double mutant N41D N281D over the WT could not be easily explained by differences in the pH-activity curves, potential structural differences were investigated. The four recombinant enzymes were analysed using circular dichroism (CD) spectroscopy (Figure 9, Table 3), which showed a substantial difference between enzymes containing the N41D mutation (N41D and the double mutant) and those without this mutation. The data suggest that the N41D mutation has structurally altered the existing α-helix in this region to make it more detectable, as demonstrated by the increased signal compared to both WT and N281D at 222nm. Using the deconvoluted

CD data, there appears to be a correlation between k_{cat} and the increase in α-helical content conferred by the N41D mutation, but no apparent correlation of the CD structural analysis (α-helix or β-sheet) with differences observed in the K_m of the various mutants. This suggests that the N41D mutation affects turnover but not substrate affinity, and given the location of this mutation near to the active-site loop, these results may make physical sense. Changes to CD spectra have been shown to correlate with differences in EcA catalytic constants previously, with fatty-acid L-asparaginase conjugates showing lowering of both Km and β-sheet content compared to the native enzyme [42]. Further, increases in β-sheet and decreases in α-helical content have been shown to correlate with decreased activity for ErA [43].

Therefore, to further understand the structural differences observed by CD in these ErA mutants, published crystal structures from the Protein Data Bank (PDB) were used (entries 1O7J, 1HG1 and 1HFW) [6, 7, 8] with the CHIMERA molecular visualisation software. Hydrogen bonding opportunities were calculated using the CHIMERA software which is based on published methods [44]. Rotamers chosen for analysis were the most probable conformations based on probability, hydrogen bonding and avoidance of clashes using the methods of Dunbrack [45]. Interestingly, both mutations appear to result in a slightly lower number of hydrogen bonds in the surrounding structural microenvironment. The N41D mutation (Figure 10A) results in loss of a hydrogen bond between the Asn_{41} sidechain amide and the peptide bond carbonyl group of Asp_{37}. This change may slightly slacken the position of the α-helix, potentially causing greater mobility of the flexible active site lid-loop which is N-terminal to this helix. This structural possibility would be consistent with the observed increase in the catalytic turnover of the N41D mutant as evidenced by the increase in k_{cat}.

The N281D mutation (Figure 10B) may also cause loss of a hydrogen bonding opportunity with one of the other chains (in the Figure, Chains A and C are shown) in the tetrameric enzyme structure. In the WT enzyme, the sidechain amide of Asn_{281} forms a hydrogen bond with the peptide carbonyl group of Ala_{171} on the opposite protein monomer. Considering that, in the case of the tetrameric assembly, this effect will occur four times in the mutant compared with the WT, it is possible that the N281D mutant tetramer is held together with slightly less strength, resulting in a slightly slacker structure. As each active site in the ErA tetramer involves residues from two separate chains, it is possible that the slightly looser tetrameric structure resulting from the N281D mutation results in a slightly wider entrance to the active site, which would be consistent with the observed increase in the K_m (as well as the consequent decrease in substrate affinity, thermal stability and denaturing stability) for the N281D mutation.

The published EwA crystal structure [30] was consulted to further understand the structural effects of the two mutations in ErA. EwA is an enzyme with 79% identity to ErA, from a very similar organism, and is a good basis of comparison from a structural point of view. Using PDB entry 2JK0 and the Chimera molecular viewing software, the structural hydrogen bonding environments around these two amino acid positions were studied. In comparison with wild type ErA, which has two hydrogen bonds originating at position 41 as described above, in EwA there is only one hydrogen bond between the peptide bond nitrogen at position 41 (Gln_{41}) and the peptide bond oxygen at position 37 (Glu_{37}). EwA lacks the additional hydrogen bond observed in WT ErA between the side chain of residue 41 and the peptide-bond oxygen of position 37, making EwA structurally more like the ErA N41D mutant. This may help explain why the ErA N41D mutation results in a higher k_{cat} compared with ErA WT, as the EwA k_{cat} is also higher than ErA WT at $1600s^{-1}$ [46]. Furthermore, at position 281, the Ser residue in EwA has two

hydrogen bonds between protein chains, one originating from the peptide bond oxygen at position 281 and one originating from the Ser_{281} sidechain. The ErA wild type enzyme has three hydrogen bonds from position 281, reducing to two in the N281D mutant, making EwA more like the ErA N281D mutation in terms of the number of hydrogen bonds in this region. The reported value of EwA K_m is 98μM [46], and the observation that at position 281 EwA is structurally akin to ErA N281D correlates with the observed difference in K_m between the N281D and WT ErA enzymes. Furthermore, the number of hydrogen bonds at this site (3 in ErA WT, 2 in ErA N281D and EwA) appears to correlate with the lower glutaminase activity [47] and decreased stability both observed for EwA [30], which like N281D was less stable at urea concentrations greater than 1.5M and temperatures greater than 45ºC.

The empirical findings in this study appear to be further supported by analysis of the mutations using computational prediction methods. The N41D mutation was predicted to have no effect on the α-helical local structure at this site using the I-TASSER prediction tools [48, 49, 50]. A check of the effect of the N281D mutation on the binding efficiency of the monomer subunits into tetramer was also performed using the Beatmusic server [51], with the calculation run as the interaction between two dimeric subunits (AB and CD) to return the full binding effect on the overall tetrameric assembly. As may be expected, the results showed that the N281D mutation is predicted to cause a significant decrease in binding affinity ($\Delta\Delta G_{bind}$), of 3.87kcal/mol, which appears to support the hydrogen-bonding structural analysis discussed above. Finally, both mutations were run through the AUTO-MUTE prediction server [52 - 54] which calculated that neither mutation should have a deleterious effect on enzyme activity, a result that supports the overall activity data in Table 1.

4. Conclusions

In order to understand the effect of deamidation on ErA, several recombinant mutants were expressed, purified and characterised. The locations of the two mutation sites studied were both quite distal to the catalytic site of the enzyme. Surprisingly, the deamidated mutants of ErA had the same, or better, activity as the wild-type enzyme. In particular, a double mutant (N41D N281D) had increased activity and turnover compared with the wild-type. The N41D mutation alone conferred a subtle increase in turnover and the N281D mutation (alone or in concert with N41D) decreased both the stability and the substrate affinity of the enzyme. These effects may be due to subtle structural changes in the hydrogen bonding network around these mutation sites, particularly for the α-helix structure around N41D, differences in which could be detected by CD. Both mutations appear to affect the structural hydrogen bonding network of the enzyme, producing structures mimicking the closely-related EwA, which like N41D also has a higher catalytic constant and like N281D has a lower glutaminase activity and thermal stability, compared with ErA.

Study of the effects of point mutations on enzymatic structure and activity remains an activity with a significant empirical component. Recent studies on L-asparaginase from *Erwinia carotovora* [55], which has 74% identity to ErA, showed that a single mutation (Gly to Ser) in a different, α-helical region somewhat distant to the active site, significantly decreased the catalytic performance of the enzyme. Studies to address the effects of Asn to Asp deamidation by mutation analysis must therefore be carried out on a case-by-case basis.

The work presented in this paper suggests that ErA deamidation at the N41 and N281 sites should not be a concern during processing, storage or clinical use. These deamidated

variants of ErA are active and stable under normal storage conditions. Of course, deamidation content of these and other sites should still be monitored, but this work has provided scientific rationale of the true impact of deamidation on ErA activity at these particular sites. This strategy may be useful, and should be considered, as part of a holistic approach when investigating the impact of deamidation on other ErA sites, or other biopharmaceutical products.

Acknowledgements

The authors would like to thank Roger Hinton, Head of Development & Production, for facilitating these studies, Nigel Allison for advice and critical review of the manuscript, and Trevor Marks, Patrick Kanda, Richard Hesp and Michael Maynard-Smith for helpful discussions. Further thanks go to the entire Development & Production team at PHE Porton.

References

1. Beard MEJ, Crowther D, Galton DAG, Guyer RJ, Fairley GH, Kay HEM, Knapton PJ, Malpas JS, and Scott RB (1970) L-asparaginase in treatment of acute leukaemia and lymphosarcoma. *Br Med J* 1, 191–195.
2. Pieters R, Hunger SP, Boos J, Rizzari C, Silverman L, Baruchel A, Goekbuget N, Schrappe M, and Pui CH (2011) L-asparaginase treatment in acute lymphoblastic leukemia: a focus on *Erwinia* asparaginase. *Cancer* 117, 2, 238-49.
3. Vrooman LM, Supko JG, Neuberg DS, Asselin BL, Athale UH, Clavell L, Kelly KM, Laverdière C, Michon B, Schorin M, Cohen HJ, Sallan SE, and Silverman LB (2010) *Erwinia* asparaginase after allergy to *E. coli* asparaginase in children with acute lymphoblastic leukemia. *Pediatr Blood Cancer* 54, 2, 199-205.
4. Broome JD (1968) Factors which may influence the effectiveness of L-asparaginases as tumor inhibitors. *Br J Cancer* 22, 3, 595-602.
5. Wriston JC (1985) Asparaginase. *Methods Enzymol* 113, 608-618.

6. Aghaiypour K, Wlodawer A, and Lubkowski J (2001) Structural basis for the activity and substrate specificity of *Erwinia chrysanthemi* L-asparaginase. *Biochemistry* 40, 5655-5664.
7. Lubkowski J, Dauter M, Aghaiypour K, Wlodawer A, and Dauter Z (2003) Atomic resolution structure of *Erwinia chrysanthemi* L-asparaginase. *Acta Cryst D* 59, 84-92.
8. Miller M, Rao JKM, Wlodawer A, and Gribskov MR (1993) A left-handed crossover involved in amidohydrolase catalysis: crystal structure of *Erwinia chrysanthemi* L-asparaginase with bound L-aspartate. *FEBS J* 328, 3, 275-279.
9. Gervais D, Allison N, Jennings A, Jones S, and Marks T (2013) Validation of a thirty-year-old process for the manufacture of L-asparaginase from *Erwinia chrysanthemi.* *Bioproc Biosys Eng* 36, 4, 453-460.
10. Aswad DW (1995) *Deamidation and isoaspartate formation in peptides and proteins.* CRC Press, Boca Raton, FL.
11. Aswad DW, Paranandi MV, and Schurter BT (2000) Isoaspartate in peptides and proteins: formation, significance and analysis. *J Pharm Biomed Anal* 21, 1129-1136.
12. Gervais D, O'Donnell J, Sung M, and Smith S (2013) Control of process-induced asparaginyl deamidation during manufacture of *Erwinia chrysanthemi* L-asparaginase. *Process Biochemistry* 48, 9, 1311-1316.
13. Zhang T, Bourret J, and Cano T (2011) Isolation and characterization of therapeutic antibody charge variants using cation exchange displacement chromatography. *J Chromatography A* 1218, 31, 5079-5086.
14. Khawli LA, Goswami S, Hutchinson R, Kwong ZW, Yang J, Wang X, Yao Z, Sreedhara A, Cano T, Tesar D, Nijem I, Allison DE, Wong PY, Kao Y, Quan C,

Joshi A, Harris RJ and Motchnik P (2010) Charge variants in IgG1 isolation, characterization, in vitro binding properties and pharmacokinetics in rats. *mAbs* 2, 6, 613-624.

15. Laboureur P, Langlois C, Labrousse M, Boudon M, Emeraud J, Samain JF, Ageron M, and Dumesnil Y (1971) L-asparaginases from *Escherichia coli*. I. Properties of the native forms. *Biochimie* 53, 1147-56.
16. Laboureur, P., Langlois, C., Labrousse, M., Boudon, M., Emeraud, J., Samain, J. S., M.Ageron, M. A., and Dumesnil, Y (1971) L-Asparaginases *d'Escherichia coli*. II. Plurality and origin of molecular forms. Relations with the biological activity. *Biochimie* 53, 1157-1165.
17. Wagner O, Irion E, Arens A, and Bauer K (1969) Partially deaminated L-asparaginase. *Biochem Biophys Res Comm* 37, 3, 383-392.
18. Bae N, Pollak A, and Lubec G (2011) Proteins from *Erwinia* asparaginase Erwinase® and *E Coli* asparaginase 2 MEDAC® for treatment of human leukaemia, show a multitude of modifications for which the consequences are completely unclear. *Electrophoresis* 32, 1824-1828.
19. Gupta R and Srivastava OP (2004) Effect of deamidation of asparagine 146 on functional and structural properties of human lens αB-crystallin. *Investigative Ophthalmology & Visual Science* 45, 1, 206 – 214.
20. Takata T, Oxford JT, Demeler B, and Lampi KJ (2008) Deamidation destabilises and triggers aggregation of a lens protein, βA3-crystallin. *Protein Sci* 17, 1565-1575.
21. Minton NP, Bullman HMS, Scawen MD, Atkinson T and Gilbert HJ (1986) Nucleotide sequence of the *Erwinia chrysanthemi* NCPPB 1066 L-asparaginase gene. *Gene* 46, 25-35.

22. Sadler JR, Sasmor H, and Betz JL (1983) A perfectly symmetric lac operator binds the lac repressor very tightly. *Proc Natl Acad Sci USA* 80, 22, 6785-9.
23. Oehler S, Amouyal M, Kolkhof P, von Wilkcken-Bergmann B, and Müller-Hill B (1994) Quality and position of the three lac operators of *E. coli* define efficiency of repression. *EMBO J* 13, 14, 3348-55.
24. Gentz R, and Bujard H (1985) Promoters recognised by *Escherichia coli* RNA polymerase selected by function: highly efficient promoters from bacteriophage T5. *J Bacteriol* 164, 1, 70-7.
25. Lanzer M and Bujard H (1988) Promoters largely determine the efficiency of repressor action. *Proc Natl Acad Sci USA* 85, 23, 8973-7.
26. Kotzia GA and Labrou NE (2005) Cloning, expression and characterisation of *Erwinia carotovora* L-asparaginase. *J Biotechnol* 119, 309-323.
27. Lee SM, Wroble MH, and Ross JT (1989) L-asparaginase from *Erwinia carotovora*. An improved recovery and purification process using affinity chromatography. *Appl Biochem Biotechnol* 22, 1, 1-11.
28. Lowry OH, Rosbrough NJ, Farr AL, and Randall RJ (1951) Protein measurement with the folin phenol reagent. *J Biol Chem* 193, 265-275.
29. Harms E, Wehner A, Jennings MP, Pugh KJ, Beacham IR and Röhm KH (1991) Construction of expression systems for *Escherichia coli* asparaginase II and two-step purification of the recombinant enzyme from periplasmic extracts. *Prot Expr Purif* 2, 144-150.
30. Papageorgiou AC, Posypanova GA, Andersson CS, Sokolov NN and Krasotkina J (2008) Structural and functional insights into *Erwinia carotovora* L-asparaginase. *FEBS J* 275, 4306-4316.

31. Whitmore, L. and Wallace, B.A. (2008) Protein Secondary Structure Analyses from Circular Dichroism Spectroscopy: Methods and Reference Databases. *Biopolymers* 89, 392-400.
32. Whitmore, L. and Wallace, B.A. (2004) DICHROWEB: an online server for protein secondary structure analyses from circular dichroism spectroscopic data. *Nucleic Acids Research* 32, W668-673
33. Lobley, A., Whitmore, L. and Wallace, B.A. (2002) DICHROWEB: an interactive website for the analysis of protein secondary structure from circular dichroism spectra. *Bioinformatics* 18, 211-212.
34. Sievers F, Wilm A, Dineen D, Gibson TJ, Karplus K, Li W, Lopez R, McWilliam H, Remmert M, Söding J, Thompson JD, Higgins DG (2011) Fast, scalable generation of high-quality protein multiple sequence alignments using Clustal Omega. *Mol Syst Biol* 7, 539.
35. Gouet, P, Robert, X and Courcelle E (2003) ESPript/ENDscript: extracting and rendering sequence and 3D information from atomic structures of proteins. *Nucl. Acids Res.* 31(13): 3320-3323
36. Pettersen EF, Goddard TD, Huang CC, Couch GS, Greenblatt DM, Meng EC, and Ferrin TE (2004) UCSF Chimera--a visualization system for exploratory research and analysis. *J Comput Chem* 25, 13, 1605-12.
37. Buck PW, Elsworth R, Miller GA, Sargeant K, Stanley JL, and Wade HE (1971) The batch production of L-asparaginase from *Erwinia carotovora*. *J Gen Microbiol* 65, i.
38. Tyler-Cross R, and Schirch V (1991) Effects of amino acid sequence, buffer, and ionic strength on the rate and mechanism of deamidation of asparagine residues in small peptides. *J Biol Chem* 266, 33, 22549-22556.

39. Xie M and Schowen RL (1999) Secondary structure and protein deamidation. *J Pharm Sci* 88, 1, 8-13.

40. Patel K and Borchardt RT (1990) Chemical pathways of peptide degradation. II. Kinetics of deamidation of an asparaginyl residue in a model hexapeptide. *Pharmaceut Res* 7, 703-711.

41. Lascu I, Chaffotte A, Limbourg-Bouchon B and Veron M (1992) A Pro/Ser substitution in nucleoside diphosphate kinase of *Drosophila melanogaster* (mutation killer of prune) affects stability but not catalytic efficiency of the enzyme. *J Biol Chem* 267, 12775-12781.

42. Ashrafi H, Amini M, Mohammadi-Samani S, Ghasemi Y, Azadi A, Tabandeh MR, Kamali-Sarvestani E and Daneshamouz S (2013) Nanostructure L-asparaginase-fatty acid bioconjugate: synthesis, preformulation study and biological assessment. *Int J Biol Macromol* 62, 180-187.

43. Jameel F, Bogner R, Mauri F and Kalonia D (1997) Investigation of physicochemical changes to L-asparaginase during freeze-thaw cycling. *J Pharm Pharmacol* 49, 472-477.

44. Mills JE, Dean PM (1996) Three-dimensional hydrogen-bond geometry and probability information from a crystal survey. *J Comput Aided Mol Des* 10, 6, 607-622.

45. Dunbrack RL (2002) Rotamer libraries in the 21st century. *Curr Opin Struc Biol* 12, 4, 431-440.

46. Krasotkina J, Borisova AA, Gervaziev YV and Sokolov NN (2004) One-step purification and kinetic properties of the recombinant L-asparaginase from *Erwinia carotovora*. *Biotechnol Appl Biochem* 39, 215-221.

47. Labrou NE, Papageorgiou AC and Avramis VI (2010) Structure-function relationships and clinical applications of L-asparaginases. *Curr Med Chem* 17, 2183-2195.

48. Zhang Y (2008) I-TASSER server for protein 3D structure prediction. *BMC Bioinformatics* 9, 40.

49. Roy A, Kucukural A, and Zhang Y (2010) I-TASSER: a unified platform for automated protein structure and function prediction. *Nature Protocols* 5, 725-738.

50. Roy A, Yang J and Zhang Y (2012) COFACTOR: an accurate comparative algorithm for structure-based protein function annotation. *Nucleic Acids Research*, 40, W471-W477.

51. Dehouck Y, Kwasigroch JM, Rooman M, and Gilis D (2013) BeAtMuSiC: Prediction of changes in protein-protein binding affinity on mutations. *Nucleic Acids Researc*h 41, W333-W339.

52. Masso M. and Vaisman I.I. (2011) A structure-based computational mutagenesis elucidates the spectrum of stability-activity relationships in proteins. *Proc. 33rd IEEE EMBC*, 3225-3228.

53. Masso M. and Vaisman I.I. (2011) Structure-based prediction of protein activity changes: assessing the impact of single residue replacements. *Proc. 33rd IEEE EMBC*, 3221-3224.

54. Masso M. and Vaisman I.I. (2010) AUTO-MUTE: web-based tools for predicting stability changes in proteins due to single amino acid replacements. *Protein Eng Des Sel* 23, 683-687.

55. Kotzia GA and Labrou NE (2013) Structural and functional role of Gly281 in L-asparaginase from *Erwinia carotovora*. *Prot Pept Lett* 20, 1302-1307.

FIGURES

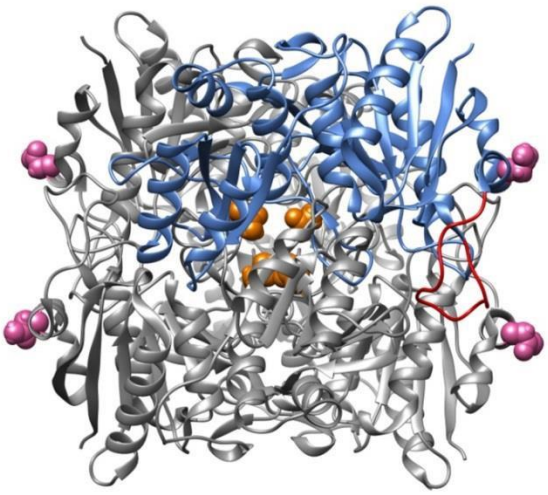

(A)

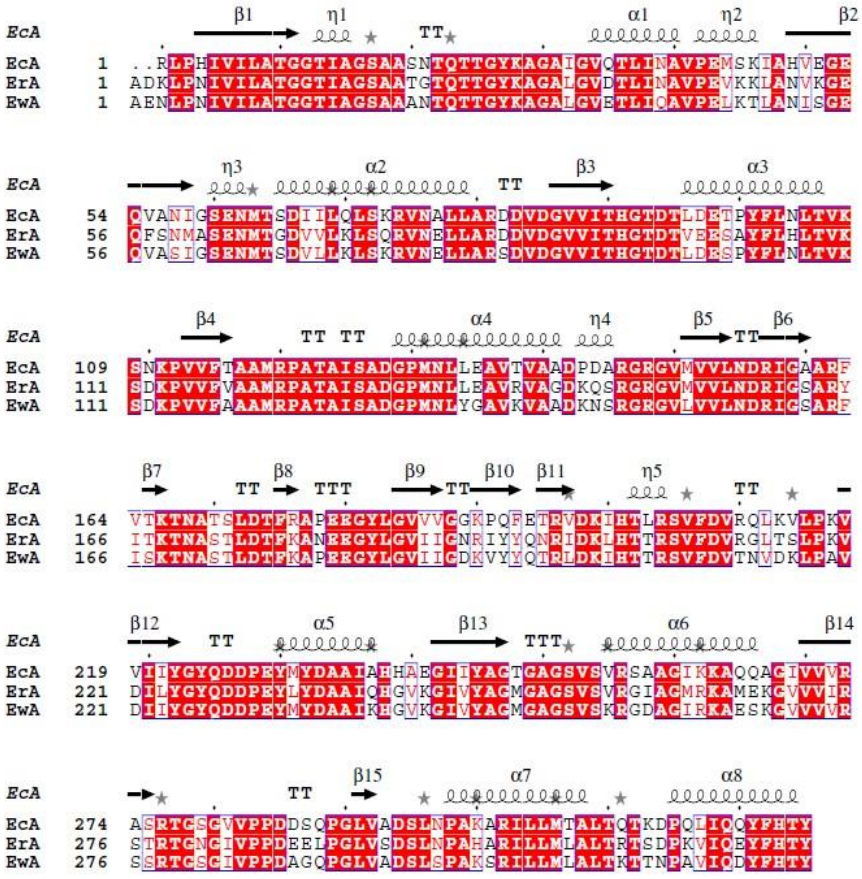

(B)

Figure 1. Structural Details of ErA Mutants. (A) Location of N41D and N281D mutations in ErA tetramer. The image was created using PDB structure file 1O7J and CHIMERA molecular viewing software. One of the four subunits is shown in blue and the other three are shown in grey. The location of the flexible lid-loop for the blue subunit is shown in red. The location of N41 is shown in pink, and the location of N281 is shown in orange. (B) Sequence alignments of ErA, EcA and EwA made using Clustal Omega and depicted using Espript. The sequence alignment is annotated with secondary structure features from PDB file 1O7J.

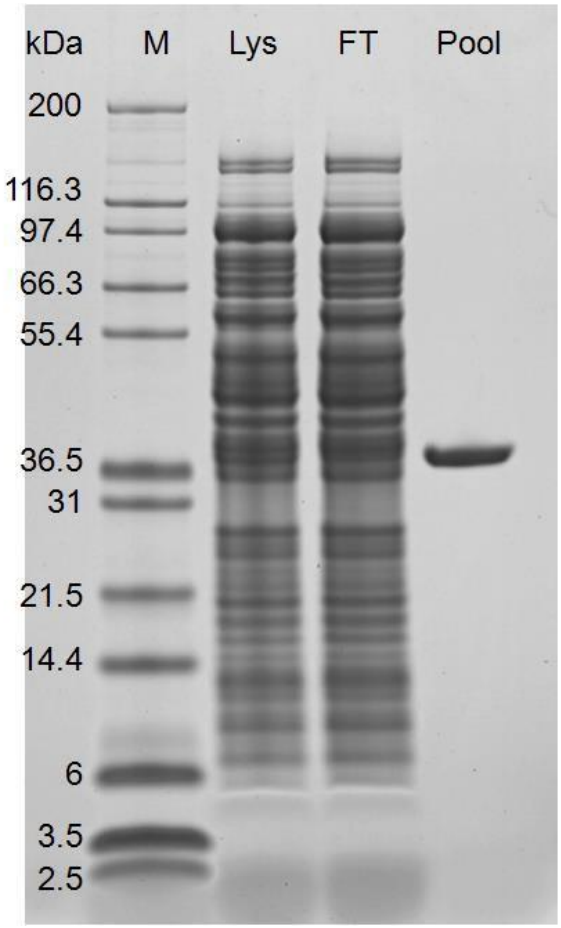

Figure 2. Purification of Recombinant ErA WT Enzyme. M – Mark12™ molecular weight marker; Lys – Cleared Lysate; FT – Chromatography Flow Through; Pool – Chromatography Enzyme Pool.

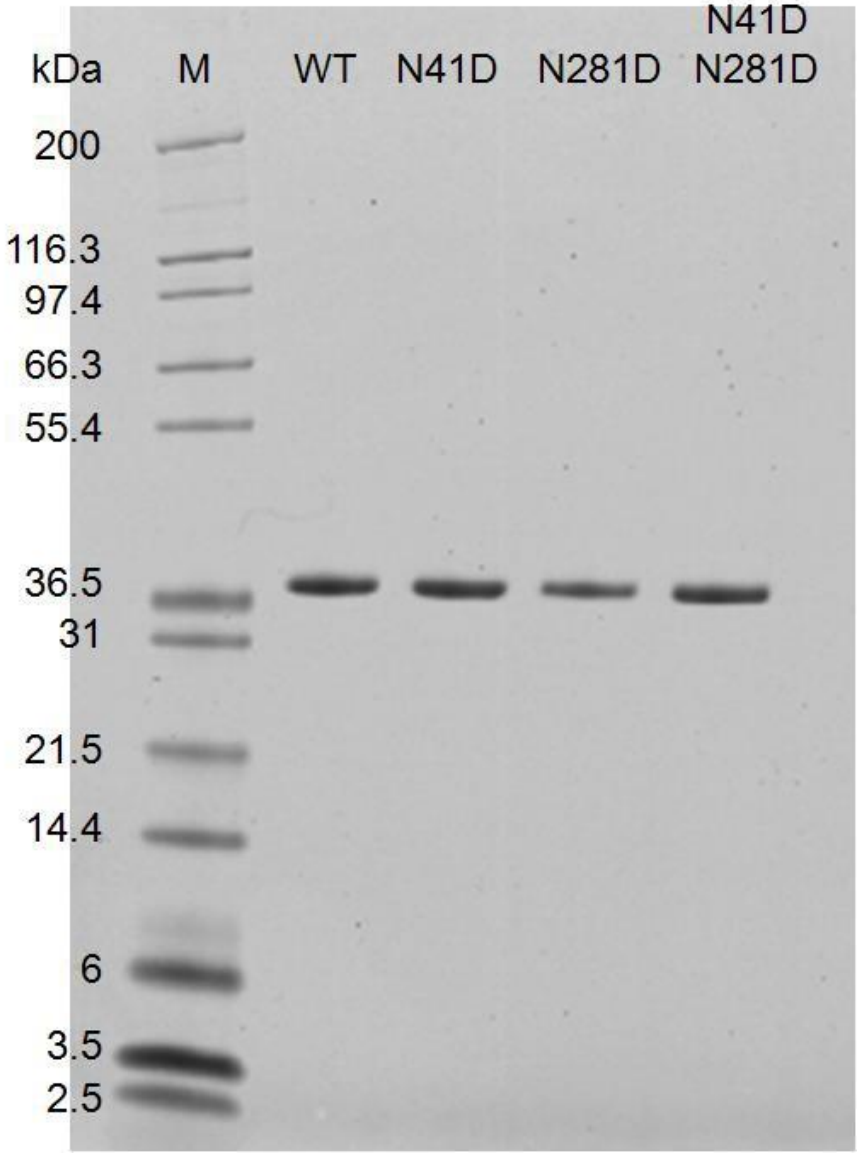

Figure 3. SDS-PAGE Analysis of Final Recombinant ErA Enzymes. The enzyme loading per well was 0.5µg/mL as judged by A_{280} protein concentration.

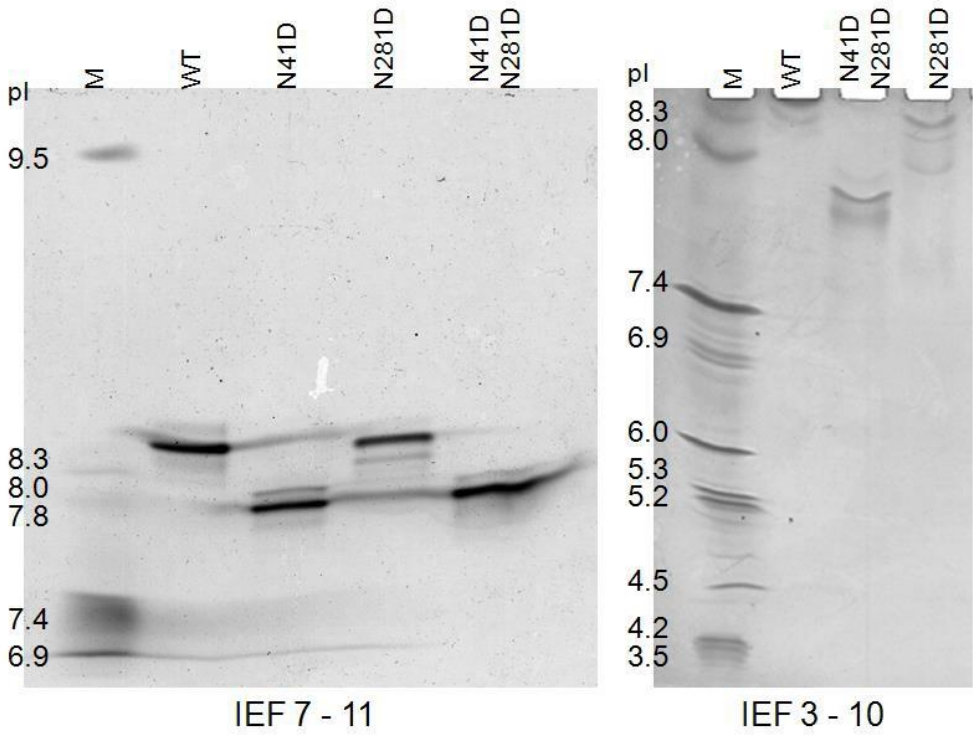

Figure 4. Isoelectric Focussing Analyses of Recombinant Deamidated ErA Mutants. M – Serva 3 – 10 pI Marker.

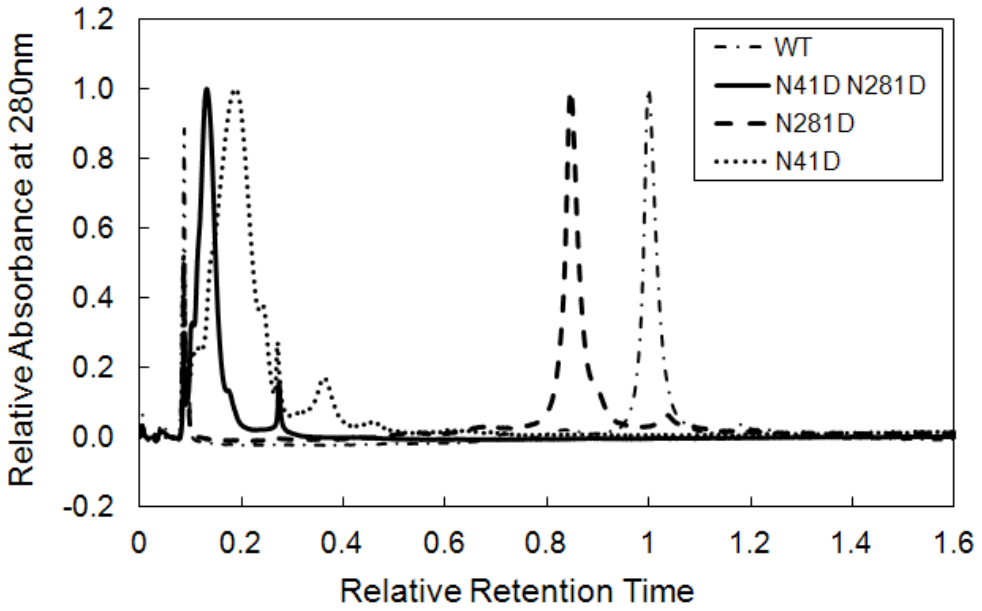

Figure 5. Weak Cation-Exchange HPLC Analyses of Recombinant ErA Mutants. The data are presented as traces using Relative Absorbance (normalised to the main-peak maximum) and Relative Retention Time (normalised to the main-peak retention of the WT enzyme).

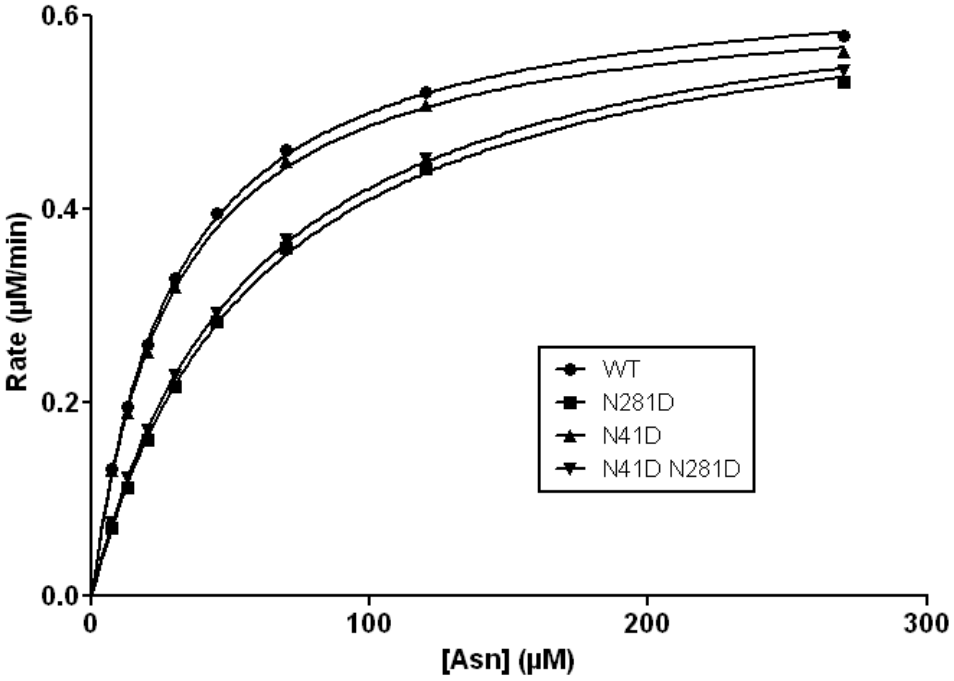

Figure 6. Michaelis-Menten plots. Eight data points at different substrate concentrations were generated for each recombinant enzyme. One outlier has been excluded for N41D. The R^2 values, indicating goodness of fit, were: WT 0.9995, N41D 0.9995, N291D 0.9993, and N41D N281D 0.9998.

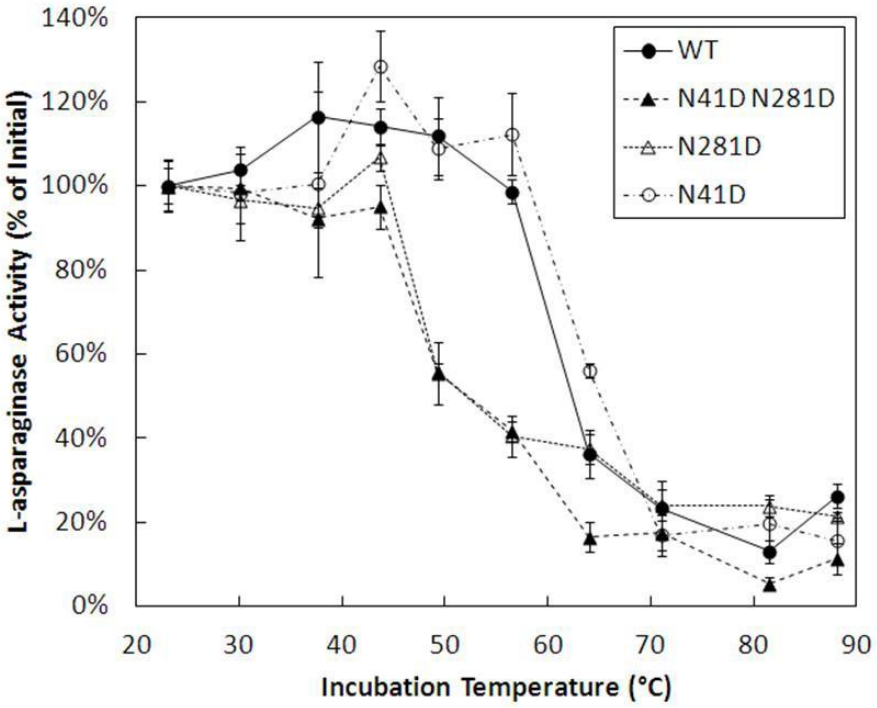

(A)

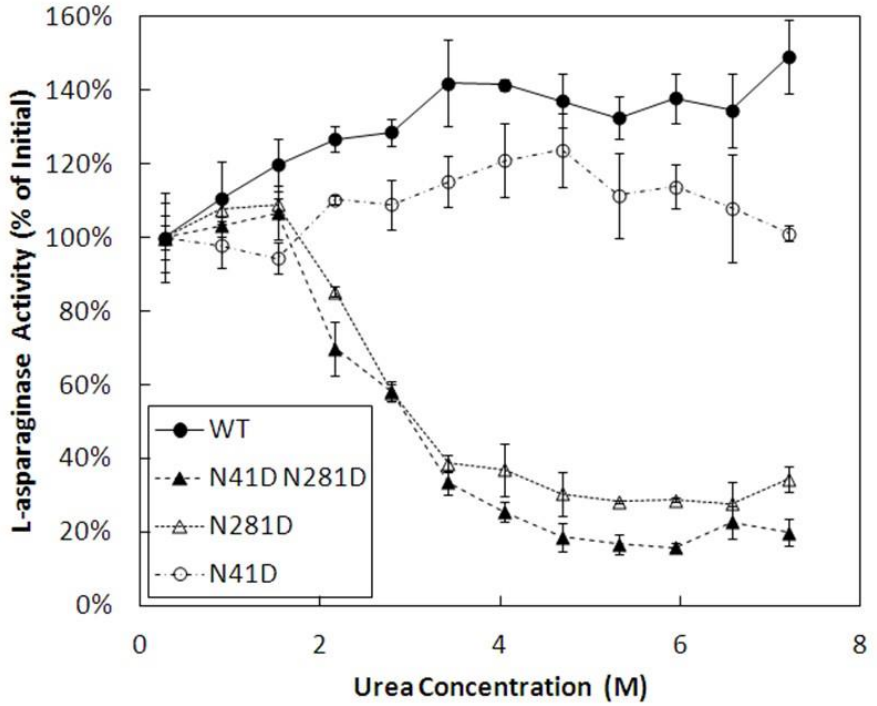

(B)

Figure 7. Stability Profiles of ErA WT and Mutant Enzymes. The data are presented as residual remaining activity after exposure to thermal stress (A) or denaturation in urea (B).

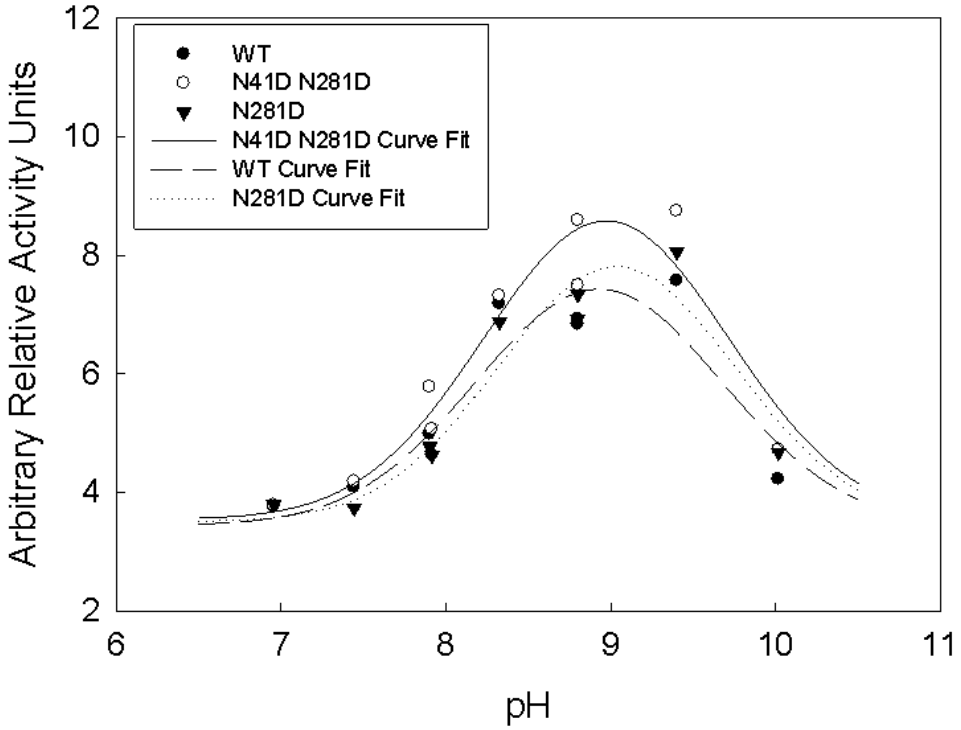

Figure 8. Effect of pH on Activity of Recombinant ErA Mutants.

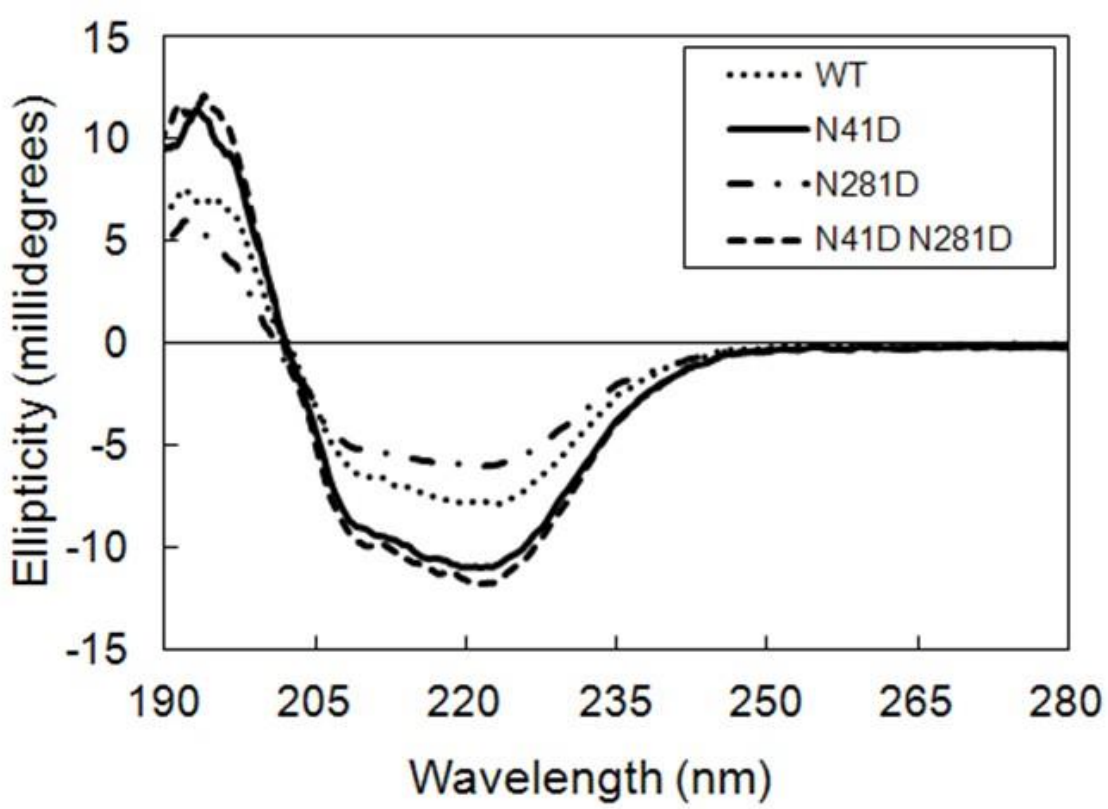

Figure 9. Circular Dichroism Spectra. The data are presented as spectra with the solvent background (analytical-grade water) subtracted.

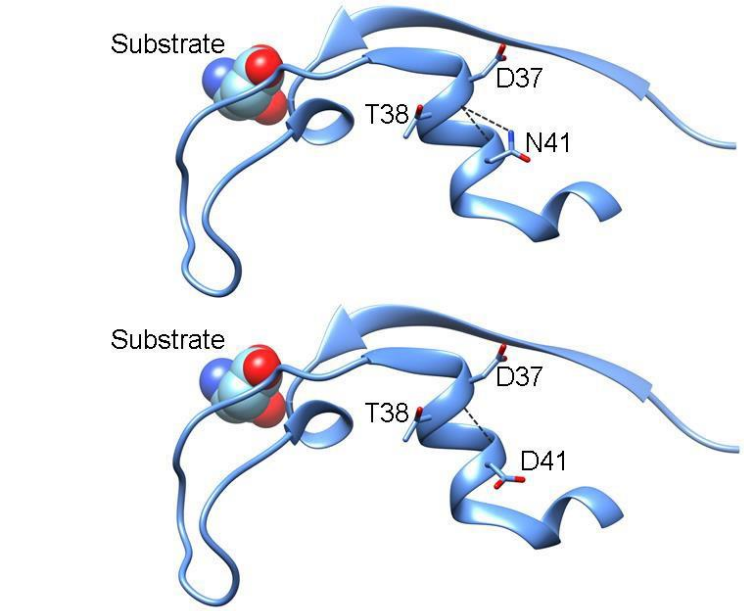

(A)

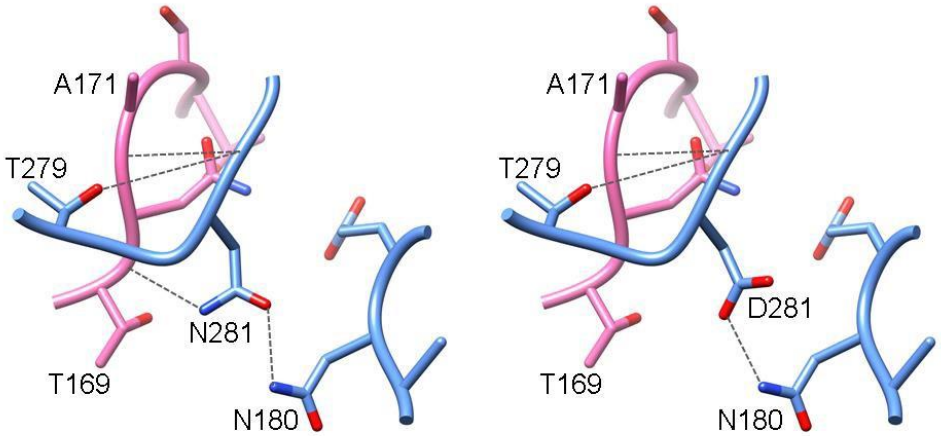

(B)

Figure 10. Hydrogen Bonding of ErA Mutations. (A) N41 Site in both Mutant and WT Enzymes. Only the hydrogen bonds originating from position 41 are depicted (by dashed lines) for both the WT (N41) and mutant (D41). The position of the substrate (here D-aspartate) is shown for reference. (B) Only the hydrogen bonds originating from position 281 are depicted (by dashed lines) for both the WT (N281) and the mutant (D281). The A-chain of the tetramer is shown in blue, and the C-chain of the tetramer is shown in pink.

Table 1. L-Asparagine Activity and Specific Activity and Glutaminase Activity of Recombinant ErA Deamidated Mutants. For L-Asn as a substrate, each activity data point represents the mean of six separate observations (measured on two different days each in triplicate). The relative standard deviation (RSD) for all L-Asn activity observations is also shown, for each enzyme. For L-Gln as a substrate, glutaminase data are reported as a ratio to asparaginase activity.

Enzyme	L-Asn Specific Activity (U/mg)	L-Asn Activity (U/mL)	L-Asn Activity RSD (%)	L-Gln Activity (Ratio to L-Asn Activity, %)
WT	908	698 (n=6)	1.5%	4.5%
N41D	1062	1072 (n=6)	2.0%	4.1%
N281D	924	776 (n=6)	3.3%	1.9%
N41D N281D	1261	1551 (n=6)	2.0%	1.8%

Table 2. K_m and k_{cat} Data for Recombinant ErA Deamidated Mutants. Data shown are for the substrate L-Asn. Confidence limits refer to a non-linear regression fit to a single data set. Purified native ErA was also tested twice for reference, giving K_m values of 28.9 and 31.5 µM with k_{cat} values of 647 and 646 s^{-1} respectively.

Enzyme	K_m (µM)	K_m 95% confidence limits (µM)	k_{cat} (s^{-1})	k_{cat} 95% confidence limits (s^{-1})
WT	29.1	27.8 - 30.4	565	556 - 574
N41D	29.1	27.6 - 30.7	657	646 - 669
N281D	59.7	55.6 - 63.8	573	557 - 590
N41D N281D	56.2	54.2 - 58.3	798	786 - 810

Table 3. CD Deconvolution Results using DICHROWEB.

Enzyme	α-Helix Content (%)	β-Sheet Content (%)	Turns (%)	Unstructured (%)
WT	21	23	19	38
N41D	37	12	20	32
N281D	15	26	18	41
N41D N281D	36	13	20	32